GRUPPO NAZIONALE DI GEOFISICA DELLA TERRA SOLIDA

35° CONVEGNO NAZIONALE

RIASSUNTI ESTESI DELLE COMUNICAZIONI

LECCE
22-24 novembre 2016

CASTELLO CARLO V

ISTITUTO NAZIONALE DI OCEANOGRAFIA E DI GEOFISICA SPERIMENTALE

EAGE EUROPEAN ASSOCIATION OF GEOSCIENTISTS & ENGINEERS — SEG — ITALIAN SECTION
16° CONVEGNO NAZIONALE

UNIVERSITÀ DEL SALENTO

ibam ISTITUTO PER I BENI ARCHEOLOGICI E MONUMENTALI

THE ROLE OF FAULT AND SLOPE INSTABILITY ON DIRECTIONAL SITE EFFECTS OBSERVED AT SANTA CATERINA, CATANIA

F. Panzera, M.S. Barbano, G. Marletta, G. Lombardo
Dipartimento di Scienze Biologiche, Geologiche e Ambientali, Università di Catania, Italy

Introduction. We show the results of an integrated study of geomorphology and seismic site response in the southern segment of the Acireale Fault (AF, eastern flank of the M. Etna, Fig. 1).

The Santa Caterina area is affected by creep phenomena and landslides along the AF (Barbano *et al.,* 2014). We carried out measurements of ambient noise using the Horizontal-to-Vertical Spectral Ratio (HVSR) technique, in order to infer the occurrence of directional amplification effects in the fault zone.

The fractures analysed in this study took place along the AF tectonic escarpment, belonging to a wider system, locally known as Timpe system (Azzaro *et al.,* 2012). The Timpe fault system displaces a large part of the Etna eastern flank by a 20-km-long and 5-km-wide belt of transtensive structures, striking from N–S to NW–SE (Fig. 1). Faults are organized in series of parallel east-facing steep faults, segmented into individual steep fault escarpments up to 5–8 km long and up to 200 m high, offsetting late Pleistocene to Holocene volcanics and historical lava flows (Branca *et al.,* 2011). The AF runs for 6.5 km from Capo Mulini (south of Acireale) to S. Tecla (north of Acireale), controlling the roughly N–S oriented coastal line (Fig. 1). A steep cliff up to 120 m high characterizes the fault. Near S. Caterina a short N–S trending graben is developed as the result of gravity-induced effects typically occurring on the footwall of high oversteepened escarpments (Branca *et al.,* 2011). Another minor graben is produced by two minor NE–SW faults at S. Caterina village (Fig. 1d). A detailed field survey was performed in the area to map the main coastal instability features (Barbano *et al.,* 2014).

The accumulate deformation in the Timpe fault system is relapsed with stickslip motion, producing seismic sequences of low magnitude (M<4.9) and with aseismic displacements on nearby faults.

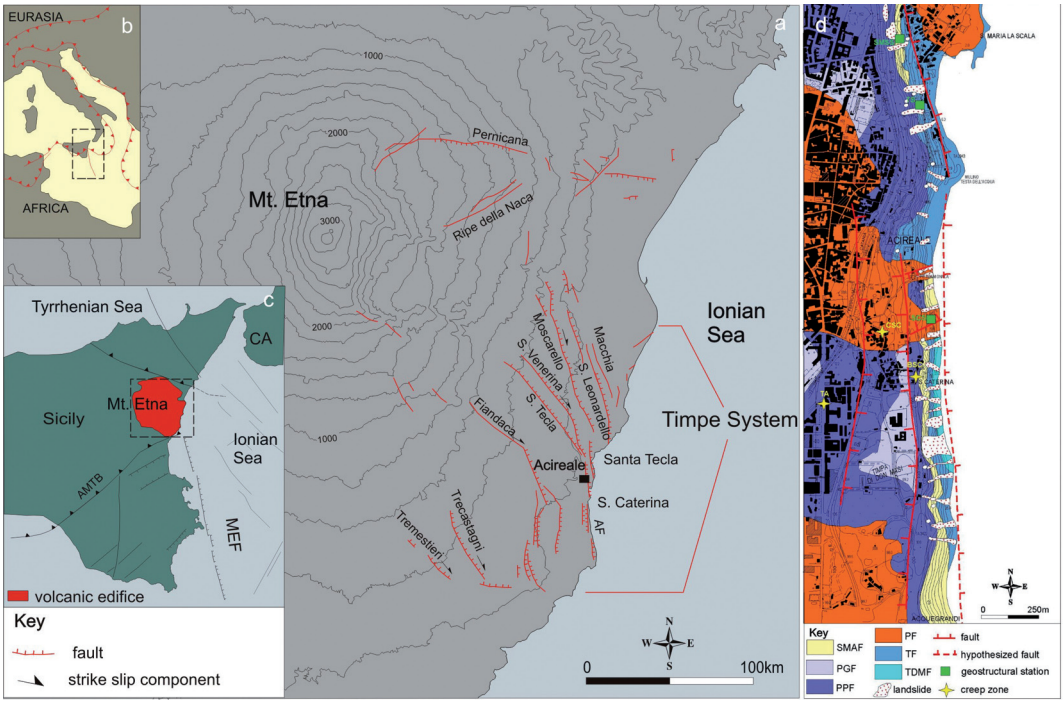

Fig. 1 – a) Tectonic framework of Mount Etna; the black rectangle to the South of Acireale shows the location of Fig. 1d. Inset b) shows location and the Africa–Eurasia plate configuration; inset c shows the main domains and structural elements of eastern Sicily: CA Calabrian arc, AMTB Apennine–Maghrebian thrust belt, MEF Malta escarpment fault system; dashed rectangle shows the location of Fig. 1a. d) Geological map and landslides distribution in the area of Acireale Fault. TDMF Timpa di Don Masi Formation (S. Caterina member), TF Timpa Formation, PF Pietracannone Formation, PPF Piano Provenzana Formation, PGF Portella Giumenta Formation, SMAF Santa Maria Ammalati Formation. Creep zone: CSC S. Caterina, TA Acireale Terme, BSC S. Caterina' Belvedere (modified from Barbano *et al.*, 2014).

We surveyed AF along the segment of our study area and observed that the fault trace is marked by creep-induced damage to man-made features occurring along the fault strike. The NNW–SSE S. Caterina fracturing zone moved during several creep episodes. The pink house (Fig. 2a) depicted in the picture was restored several times during the last decade as well as the chapel (Fig. 2b and Fig. 2d), but recent creep movements again fractured them. Other recent creep phenomena were observed at via Pianeto and near the Camping (Fig. 2 e and Fig. 2e).

Creep rates, obtained from analysis of historical records and field survey on 16 sites along the Timpe fault systems (Rasà *et al.*, 1996), vary considerably from 0.5 to 2.3 cm/year. The authors found that two different type of aseismic slip are recognized: (1) a near-continuous, long period movement along some aseismic segments of faults and (2) intermittent, short-lived, pre and post-seismic movement related to seismically active fault segments.

Method. For the HVSR analysis, we recorded ambient noise at 30 sites (Fig. 3a) using a 3-component seismometer (Tromino). Time series of ambient noise, having a length of 30 minutes, were recorded with a sampling rate of 128 Hz and, following the guidelines suggested by the SESAME project (2004) they were divided in different time windows of 20 s each not overlapping each other. A 5% cosine taper was applied to each window and the Fourier spectra were calculated. The spectra of each window were smoothed using a Konno-Ohmachi window (Konno and Ohmachi, 1998) fixing the parameter *b* to 40. Finally, the resulting HVSR, in the frequency range 0.5-20.0 Hz, was computed estimating the logarithmic average of the spectral ratio obtained for each time window, selecting only the most stationary and excluding transients associated to very close sources.

Fig. 1 – Belvedere Place in the S. Caterina village (see Fig. 2 for location), affected by NNW–SSE fractures along: a) the floor and the house; b) the floor and the chapel; c) a wall to the north of the chapel (photographs October 4, 2012, after Barbano *et al.*, 2014); d) the same chapel and e) via Pianeto (photographs 15 September 2016).

Experimental spectral ratios were also calculated after rotating the NS and EW components of motion by steps of 10 degrees starting from 0° (north) to 180° (south). This approach, first applied to earthquake recordings in studying the directional effects due to topographic irregularities at Tarzana, California (Spudich *et al.*, 1996), has been used for ambient noise signals by several authors to identify site response directivity in the presence of faults (e.g. Panzera *et al.*, 2016 and reference therein).

In this study we also apply the time-frequency (TF) polarization analysis proposed by Vidale (1986) and exploited by Burjánek et al. (2012 and reference therein). This technique can provide quite robust results, overcoming the bias that could be introduced by the denominator spectrum in the HVSR calculation. Following Burjánek et al. (2012 and reference therein), the continuous wavelet transform (CWT) is applied to signals in order to select time windows whose length matches the dominant period: signals are thus decomposed in the time-frequency domain and the polarization analysis is applied. For each time-frequency pair, polarization is characterized by an ellipsoid and is defined by two angles: the strike (azimuth of the major axis projected to the horizontal plane from North) and the dip (angle of the major axis from the vertical axis). Another important parameter is ellipticity that is defined, according to Vidale (1986), as the ratio between the length of the minor and major axes: this parameter approaches 0 when ground motion is linearly polarized. Polarization strike and dip obtained all over the time series analyzed are cumulated and represented using polar plots where the contour scale represents the relative frequency of occurrence of each value, and the distance to the center represents the signal frequency in Hz. In order to assess whether ground motion is linearly polarized, the ellipticity is also plotted versus frequency.

Results and Discussion. We focused the present study on the part in which there is major evidence of fracturing. The HVSR measurements were performed near the cliff edge, where the fractures are more evident and moving away from it (see Fig. 3a, for measurement point's location). The HVSR results point out a clear seismic site effect very marked in the neighbourhood of the fractures, in the eastern part of the studied area, and a decrement moving towards West. In particular, the HVSRs show a tendency to increase the amplitude, in the frequency range 1.5-4.0 Hz, with a clear "eye shape" in the FFT (e.g. Figs. 3b and 3c). The presence of a clear "eye shape" allowed us to exclude anthropic disturbance on HVSR results. The rotated spectral ratios (e.g. Fig. 3d) show a broadband frequency effect with several adjacent peaks pointing out a preferential direction, which is the typical behavior of directional resonances. In particular, such effects are with angles of about 80°-90°. The results coming out from the use of TF

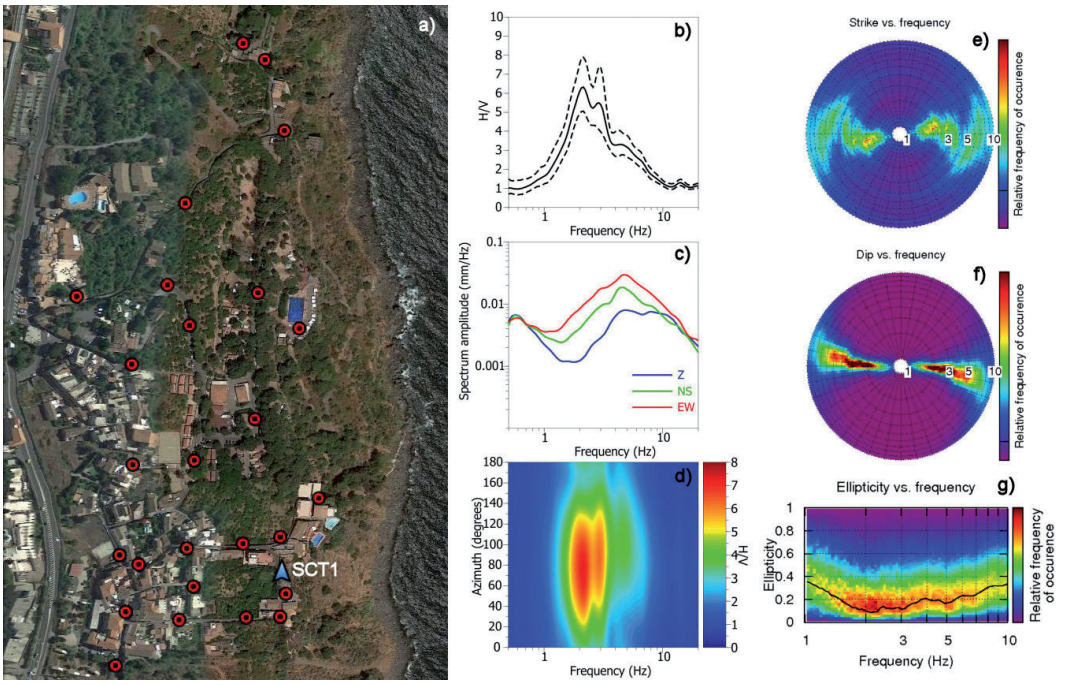

Fig. 1 – Location of the ambient noise measurements, SCT1 is the location of the measurement site shows as example (a); Example of HVSR (b), FFT (c), rotate HVSR (d), polarization polar plot (e), strike polar plot (f) and ellipticity (g) results obtained at SCT1 site, located in the fractured zone.

method allowed us to better quantify the horizontal polarization of the ground motion, giving a clear indication that ambient noise is affected by a significant horizontal polarization at the measurement sites along and across the investigated faults. It is indeed interesting to observe that the recorded ambient noise is polarized in a narrow frequency band (1.0-4.0 Hz), following a roughly east-west trend (e.g. Fig. 3e) that is almost perpendicular to the fault strike.

Moreover the TF polarization analysis revealed values of the ellipticity reaching a minimum in a wide frequency band (1.0-4.0 Hz) as well as dip values showing an horizontal trend in the same frequency band (see examples in Figs. 3f and 3g). We stress that in this area geological investigation found clear evidence of the presence of the fault, as fractures on buildings and concrete road walls.

It is clear that the maxima of the horizontal polarization occur in the north-east to east-north-east direction, although in some cases the high frequency directionality is more complex. As observed by Burjánek et al. (2010), high-frequency ground motion can indeed be controlled by the vibration of smaller blocks that imply both different resonant frequencies and directions.

Burjánek *et al*. (2012 and reference therein) point out that the ambient noise polarization takes place at about 90 degree angle to the observed fractures which are perpendicular to the sliding direction. In the present study, the polarization angle is parallel to the opening cracks, which appears in contrast to the above mentioned results. A possible explanation of our findings is that there exists a prevailing north-easterly sliding direction of the landslide body, which is strongly affecting the polarization direction especially in the 1-10 Hz frequency range.

Conclusions. Ambient noise measurements performed along the southern segment of the Acireale Fault pointed out directional amplifications that are also confirmed by the results of the time–frequency analysis, the largest amplification occurring with high angle to the fault strike. The nature of the observed site effects is highly complex as a number of different mechanisms, such as near-surface structures and slow gravitational deformations, contribute. Consequently,

the shear wave velocities could be reduced with respect to the values typical of lava formations. Measurements performed some hundreds meters away from the fault zone show a reduction of the observed directional effects that may be ascribed to the fault fabric. We relate the polarization effect to compliance anisotropy in the fault zone, where the presence of predominantly oriented fractures makes the normal component of ground motion larger than the transversal one. Such findings corroborate the hypothesis that the observed landslide movements can be related to creep movements along the investigated fault.

References

Azzaro R., Branca S., Gwinner K. and Coltelli M.; 2012: *The volcano-tectonic map of Etna volcano, 1:100.000 scale: an integrated approach based on a morphotectonic analysis from high-resolution DEM constrained by geologic, active faulting and seismotectonic data*. Ital. J. Geosci., 131 (1), 153–170. DOI: 10.3301/IJG.2011.29.

Barbano M.S., Pappalardo G., Pirrotta C. and Mineo S.; 2014: *Landslide triggers along volcanic rock slopes in eastern Sicily (Italy)*. Nat. Hazards, **73** (3), 1587-1607, doi: 10.1007/s11069-014-1160-1.

Branca S., Coltelli M., Groppelli G. and Lentini F.; 2011: *Geological map of Etna volcano*, 1:50,000 scale. Ital. J. Geosci., **130** (3), 265-291.

Burjánek J., Moore J. R., Molina F. X. Y. and Fäh D.; 2012: *Instrumental evidence of normal mode rock slope vibration*. Geophys. J. Int., **188**, 559-569.

Konno K. and Ohmachi T.; 1998: *Ground-motion characteristics estimated from spectral ratio between horizontal and vertical components of microtremor*. Bull. Seism. Soc. Am., **88**, 228-241.

Panzera F., Lombardo G., Monaco C.; 2016: *New evidence of wavefield polarization on fault zone in the lower NE slope of Mt. Etna*. Italian Journal of Geoscience, 135(2), 250-260, doi: 10.3301/IJG.2015.22

Rasa` R., Azzaro R., Leonardi O.; 1996: Aseismic creep on faults and flank instability at Mount Etna volcano, Sicily. Geol. Soc. London Spec. Publ. 110, 179–192.

SESAME; 2004: *Guidelines for the implementation of the H/V spectral ratio technique on ambient vibrations: Measurements, processing and interpretation*. SESAME European Research Project WP12, deliverable D23.12.

Spudich P., Hellweg M. and Lee W. H. K.; 1996: *Directional topographic site response at Tarzana observed in aftershocks of the 1994 Northridge, California, earthquake: implications for mainshock motions*. Bull. Seism. Soc. Am., **86**, 193-208.

Vidale J.E.; 1986: *Complex polarization analysis of particle motion*. Bull. Seism. Soc. Am., 76, 1393–1405.